41th AIAA Plasmadynamics and Lasers Conference AIAA-2010-4492
28 Jun – 1 Jul 2010, Chicago, IL

Improvement in Optical Environment over Turrets with Flat Window Using Passive Flow Control

Stanislav Gordeyev[*], Jacob A. Cress[†], Adam Smith[‡] and Eric J. Jumper[§]

University of Notre Dame, Notre Dame, IN, 46556

Several pin configurations were tested in an attempt to improve the aero-optical environment at large look-back angles over a cylindrical turret with a flat window. When small-diameter, tall pins were placed upstream of the cylindrical turret they created a partial blockage and formed a second shear layer. The second shear layer reduced the turbulent intensity of the main shear layer, with a reduction in the overall levels of aero-optical aberration by as much as 20% over a range of elevation angles between 120 and 145 degrees. A simple model is presented proposing a physical mechanism for the aero-optical reduction.

I. Introduction

TURRETS are the most-common devices used to transmit laser beams from airborne platforms due to their presumed large field of regard. On the other hand, a complex flow topology around turrets and associated aero-optical effects not only render the aft field of regard unusable, but present a difficult problem to study [1]. If a collimated laser beam is propagated through this turbulent field, different regions of the beam are advanced while other regions are retarded, resulting in an aberrated beam. The disruption of laser energy from the ideal diffraction-limited pattern can greatly reduce the usefulness of the laser system. When the laser is carried aboard an aircraft, there are two main causes of beam aberration; the turbulent air flow immediately around the aircraft (layer thickness on the same order or less of the beam aperture), coined the ``aero-optic'' problem by Gilbert [2], and the many orders of magnitude longer-length, atmospheric-propagation problem from the aircraft to the target. Modern beam control and adaptive optics can compensate for much of the low-frequency effects of the atmospheric problem; for aero-optic-induced beam degradation, however, the aberrations of the turbulent flow occur at frequencies on the order of kHz's, placing beam control outside of current correction capabilities. So there is much potential benefit in system performance that can be gained by using flow control (preferably passive control) to improve the flow around turrets to improve the aero-optical environment.

For a turret with a conformal window aero-optical aberrations are consistently lower than for a turret with a flat window. Also, in the case when the turret has a flat aperture window, the flow is also viewing-angle dependent. In [3] the optically aberrating environment around a generic hemisphere-on-cylinder turret with a flat window was experimentally studied at limited elevation and azimuthal angles at several subsonic Mach numbers. It was found that the flow topology and hence the physical mechanism of optical distortions strongly depends on the angle between the window plane and the incoming flow. When the flow over the flat window faces a moderate or strong adverse pressure gradient, it separates. At small look-back angles the adverse pressure gradient is localized to the geometric discontinuity at the upstream edge of the window, and the separated flow results in an unsteady separation bubble and subsequent reattached flow over the window. When the angle is sufficiently large the flow fully separates; once this happens the aberrating character of the separated shear layer is identical with that of any of experimentally-studied separated shear layers [4].

In order to better understand the underlying physics of optical aberrations in the separated region over the windows of flat-windowed turrets, a simpler experiment with a flat-windowed cylindrical turret

[*] Associate Research Professor, Department of Aerospace and Mech. Eng., Senior AIAA member.
[†] Graduate Research Assistant, Department of Aerospace and Mech. Eng., Student AIAA member.
[‡] Graduate Research Assistant, Department of Aerospace and Mech. Eng., Student AIAA member.
[§] Professor, Department of Aerospace and Mech. Eng., Fellow AIAA.

was conducted since many of the same flow characteristics are present in this configuration as on the more-complicated, flat-window hemispherical turret [5]. Also, several passive flow control devices were tested [6,7] and they were shown to reduce aero-optical effects at elevation angles between 90 and 110 degrees. The basis for the improvement was shown to be an energizing of the boundary layer that allowed the flow to resist separation of the flow over the flat-window for look-back angles less than 120 degrees. Pins were shown to also act the same way for hemispherical, flat-windowed turrets for look-back angles less than 120 degrees [7]. Above 120 degrees the flow separates even with the pins. These pins essentially brought flat window performance up to that provides by a conformal-window turret; both conformal and pin-enhanced flat-window turrets saw aero-optical separation-related effects at angles of 120 degrees and larger. At these large angles the aero-optic environment is imposed by a separated shear layer.

The current study attempts to reduce aero-optical effects at even higher elevation angles using an array of equally-spaced, vertically positioned pins, in this case to see if pins can improve the environment imposed by the shear layer. Parametric studies of the pin height, diameters and spacing were carried out and their resulting flow fields were experimentally measured using hot-wire and optical sensors. Section II provides a description of the experimental set-up. Both velocity and optical results are presented in Section III. Finally, the results are discussed and a simple model to explain these results is given in Section IV.

II. Experimental Set-up

All tests were performed in the transonic facilities at the Hessert Laboratory for Aerospace Research, University of Notre Dame. The facilities are described in details in [8]. A test section hosting the rotating cylindrical turret was made of Plexiglas and optical glass on top of the test section for optical access. The dimensions and arrangement of the test section are shown in Figure 1. The cylindrical turret consists of a rotatable cylinder, 4 inches in diameter, with a flat window 2 inches long and 3 inches wide with an optically accessible portion of 1.5 inches by 2.5 inches. The cylinder can be rotated so the flat window can be at any back-facing angle between 90 and 150 degrees relative to the freestream direction, with 0 degrees corresponds to the upstream direction. The streamwise x-coordinate originates from the cylinder center and the crosstream *y*-coordinate is vertical with zero at the floor of the test section upstream of the turret, see Figure 1, right.

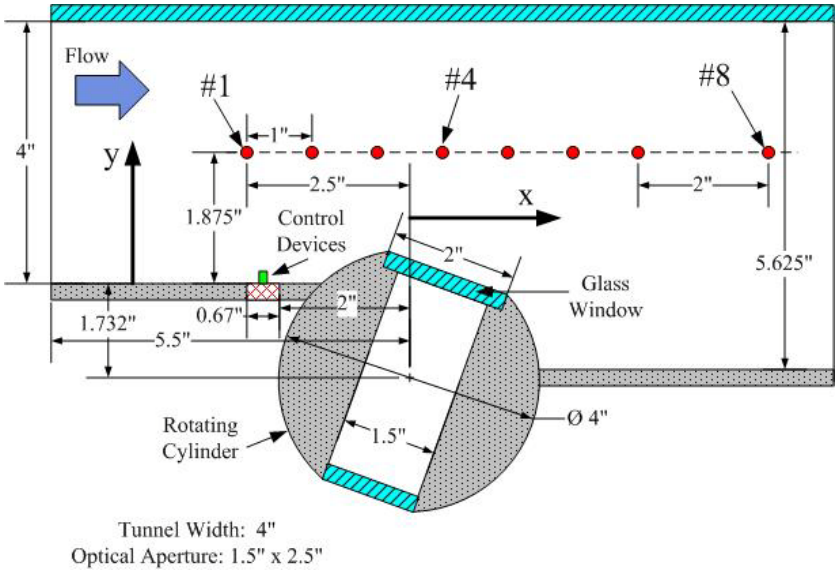

Figure 1. Dimensional drawing of the 2-dimensional turret.

The side wall of the test section is instrumented with 8 steady pressure ports to monitor the streamwise evolution of the flow around the cylinder. Ports are positioned 1” apart along a line on the side wall of the test section 2” from the upper wall.

A range of Mach numbers between 0.4 and 0.5 was selected to investigate optical aberrations over the turret. To achieve these conditions, the flow in the tunnel test section is driven by a vacuum pump with variable valve settings.

In order to measure optical distortions over the flat window insert, a commercially available CLAS-2D 2-dimensional wavefront sensor was used. A schematic of the 2-D wavefront optical set-up is presented in Figure 2, left. A round collimated laser beam, 2 inch in diameter, was steered through the flat window, normal to it, using a series of flat mirrors. A return mirror outside of the test section was used to bring the laser beam back to the optical bench along exactly the same path, thus doubling the optical distortions imprinted of the laser beam. The beam's optical distortions were measured using the CLAS-2D sensor which is a Shack-Hartmann-type wavefront sensor with a 33 x 44 lenselet array. A pulsed, frequency-double NdYAG laser was used so the sensor integration time was 6 nsec. The wavefronts were sampled at 20 Hz. Several hundred wavefronts were recorded for each elevation angle investigated between 120 and 150 degrees at a Mach number of 0.5. Piston, steady-lensing and tip/tilt components were removed from each wavefront. Levels of optical distortions were characterized by time-averaging the spatial root-mean-square of fluctuating optical wavefront, OPD_{rms}.

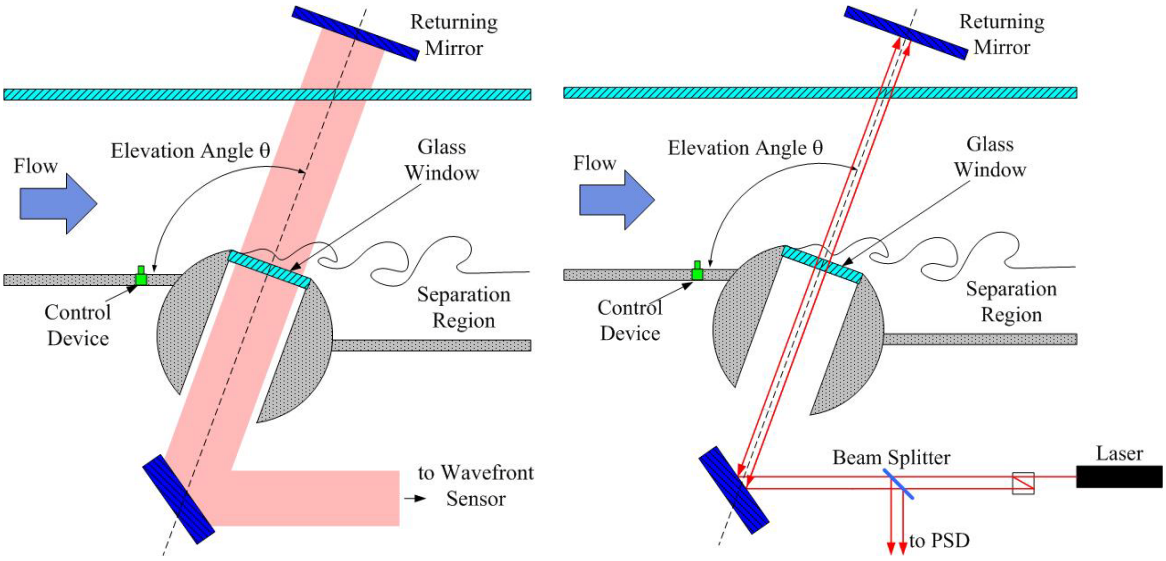

Figure 2. The optical set-up to measure wavefronts (left plot) and Malley probe set-up (right plot).

The 2-D wavefront sensor provided spatially-resolved wavefronts, but these were totally uncorrelated due to the low sampling rate. To obtain temporal information about the optical distortions over the window, a Malley probe was used. The principle of operation and detailed description of a typical Malley Probe set-up can be found elsewhere [3]. The Malley probe uses two small (~1mm in diameter) parallel laser beams closely spaced (~3-5 mm) in the streamwise direction, see the schematic set-up in Figure 2, right. Instantaneous beams' deflection angles were sampled at high sampling rates using analog Position Sensing Devices (PSD) and 1-D slices of wavefronts can be reconstructed using Taylor's frozen flow hypothesis [3]. Also, the Malley probe provides non-intrusive measurements of convective speeds of optically aberrating distortions as a function of frequency by computing spectral cross-correlation between two beams [3]. In this set-up, two parallel laser beams were positioned 4 mm apart in the streamwise direction at the center of the flat window and deflections angles were recorded for 10 sec at a sampling rate of 100 kHz.

Several passive-control, pin configurations were tested to see to whether they could affect the turbulence in the separated shear layer over the flat-window aperture in such a way that the resulting optical distortions could be decreased. Inserts with pin arrangements were placed upstream of the turret, see Figure 1. Geometrical information about all tested configurations is provided in Figure 3.

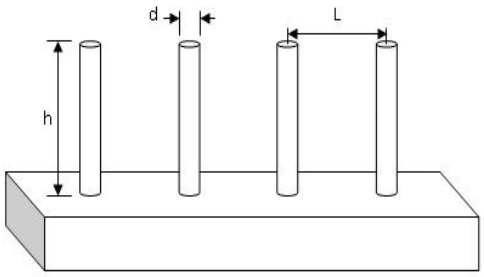

Configuration	Diameter d (mm)	Spacing L (mm)	Height h (mm)
Baseline	0	0	0
B	1	2.5	6
C	1	2.5	14
D	2	5	12
E	0.5	2.5	9
F	0.5	2.5	16
G	0.5	3.5	13
H	0.5	5	13

Figure 3. Passive Flow control Devices (pins). Left: definition of parameters, right: tested configurations.

In addition to direct optical measurements, velocity profiles in the *y*-direction were measured at several streamwise locations using a single hot-wire. The incoming freestream Mach number was M = 0.4. Velocity profiles were collected at seven streamwise locations between -0.5R and 1.0R, where R is the turret radius. Each profile was measured from the closest-to-the-wall reachable point up to y/R = 1.0 at intervals of y/R = 0.0197 using a computer-controlled traverse system. Each point was sampled at 60kHz for 5sec. Pre- and post-calibrations were performed using a Collis and Williams fit with n = 0.4. Each profile was non-dimensionalized by the incoming freestream speed. The upstream boundary layer at x/R = -1.25 upstream of the cylinder centerline had a thickness of approximately 5 mm, and a displacement thickness, δ^*, and momentum thicknesses, Θ, of 0.81 mm and 0.69 mm, respectively. The maximum boundary layer fluctuating velocity had a normalized turbulence level of 0.08.

III. Results

A. Velocity profiles

The baseline flow was fully characterized in previous investigations and the main aero-optically aberrating source was found to be a two-dimensional shear layer separated from the upstream corner of the window which formed the slope discontinuity on the turret [5,6,7]. The streamwise evolution of mean and fluctuating velocity profiles around the turret for the elevation angle of 120 degrees is shown in Figure 4. In the absence of flow-control pins, a single shear layer formed at the slope discontinuity on the turret and widened linearly over the flat window. By x/R = 1 the maximum fluctuating velocity inside the shear layer was found to be approximately 0.2 of the freestream velocity.

The streamwise evolution of the freestream velocity over the turret was measured by series of static pressure ports on the side wall of the test section, see Figure 1. The baseline results are shown in Figure 5 for all elevation angles tested. For 120 and 130 degrees, the initial portion of the cylinder before the corner worked as a ramp and deflected streamlines upward, causing the freestream Mach number to increase downstream of the turret. For elevation angles above 130 degrees the streamlines stayed parallel to the test section upper wall and Mach numbers along the test section didn't significantly change downstream. For 145- and 150-degree cases the flow slowed down after the separation. Inspection of the velocity field (not shown) revealed that the shear layer dips down after separating from the turret at these angles. One possible explanation is that the flow at these angles separates before the turret corner, so the shear layer tended to stay attached longer and developed some downward momentum.

Velocity profiles for the C pin configuration were taken at the same streamwise locations as for the baseline; these results are shown in Figure 6. The presence of the pins clearly formed a second shear layer upstream of the turret and reduced the turbulent intensity of the main shear layer down to 0.13 of the incoming freestream speed at x/R = 0.75, see Figure 7, left plot. The second shear layer began widening rapidly after it passed the turret corner and almost merged with the main shear layer by x/R = 1. Investigation of the velocity spectra at local peaks of the velocity turbulent intensities, marked by circles in Figure 7, left plot, showed that the presence of the second shear above the main one suppressed the velocity spectrum in the middle of the main shear layer for frequencies higher than 1 kHz, see Figure 7, bottom, implying that the second shear layer either suppressed the energy transfer to or amplified the energy

transfer from the small-scale, high-frequency structures in the main shear layer and thus reduced their spectral energy.

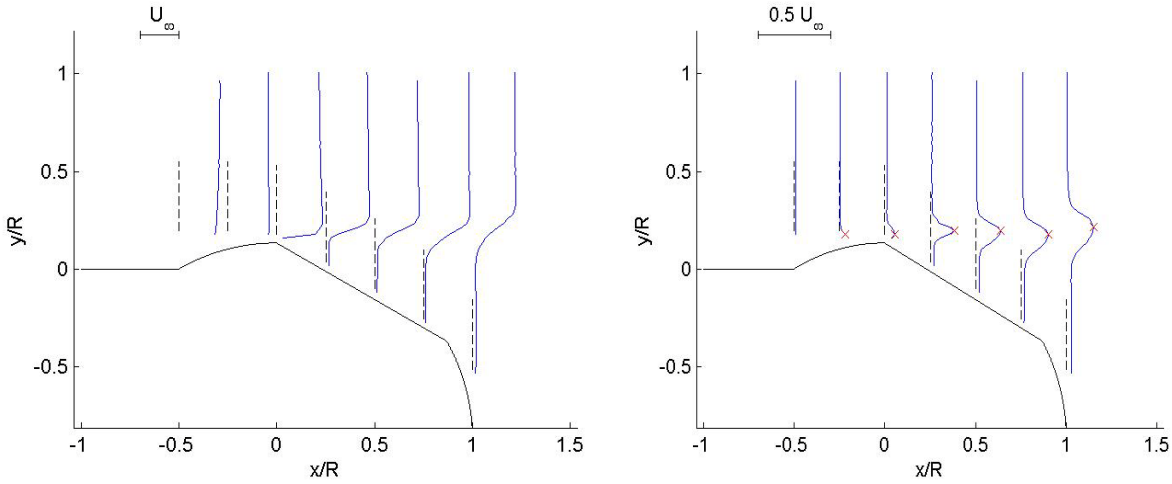

Figure 4. Normalized mean (left) and fluctuating (right) components of velocity profiles around the cylindrical turret for the baseline configuration at the elevation angle of 120 degrees. Measurement locations are marked by dashed lines. Locations of the maximum turbulent intensity are marked by x's.

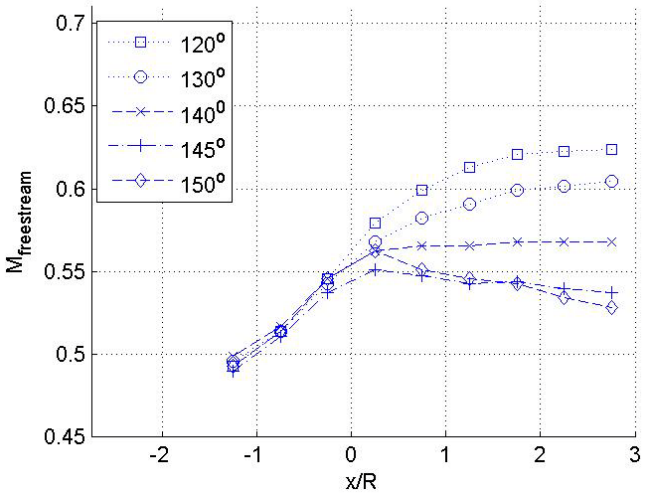

Figure 5. Mach number distribution along the test section for the baseline case at different elevation angles. Incoming M = 0.5.

Velocity profiles in the case of the F pin configuration are shown in Figure 8. These smaller-diameter pins formed a weaker second shear layer, which resulted in a reduced interaction with the main shear layer, compared to the C case. By x/R = 0.75 location, the maximum velocity fluctuation inside the main shear layer was reduced to 0.16 of the freestream speed, as opposed to the value of 0.2 for the baseline, see Figure 9, left plot. The second shear layer also suppressed the spectral energy of the main shear layer at the high end of the spectrum above 5 kHz, see Figure 9, right plot.

Comparison of the fluctuating velocity profiles at x/R = 0.75 between the baseline and the D pin configuration are shown in Figure 10, left plot. The thicker pins reduced the maximum velocity fluctuation of the main shear layer to approximately 0.15 of the freestream speed; but in addition, these pins increased the maximum intensity of the second shear layer to 0.075 of the freestream velocity.

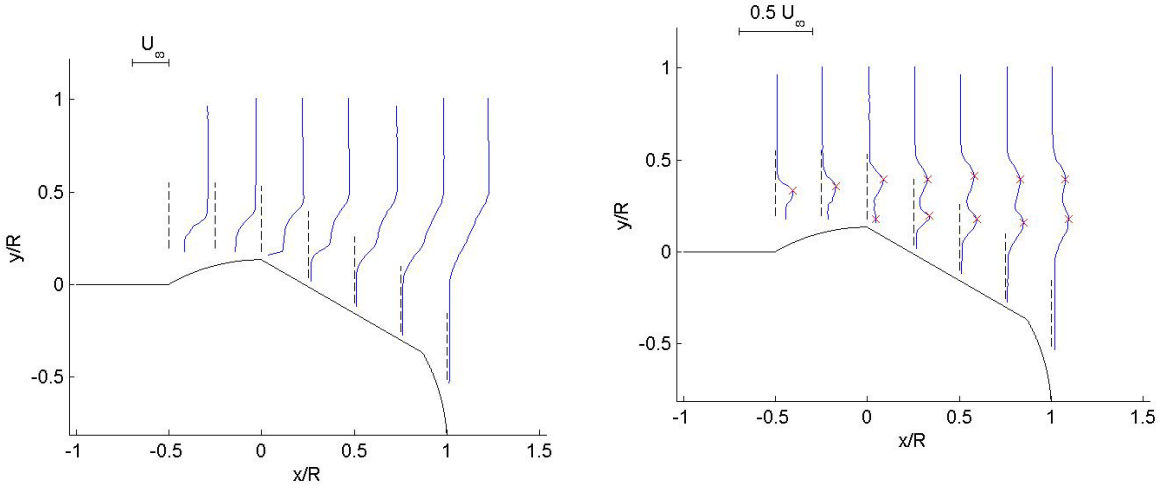

Figure 6. Normalized mean (left) and fluctuating (right) components of velocity profiles around the cylindrical turret for the C pins configuration at the elevation angle of 120 degrees. Measurement locations are marked by dashed lines. Locations of the maximum turbulent intensity are marked by crosses.

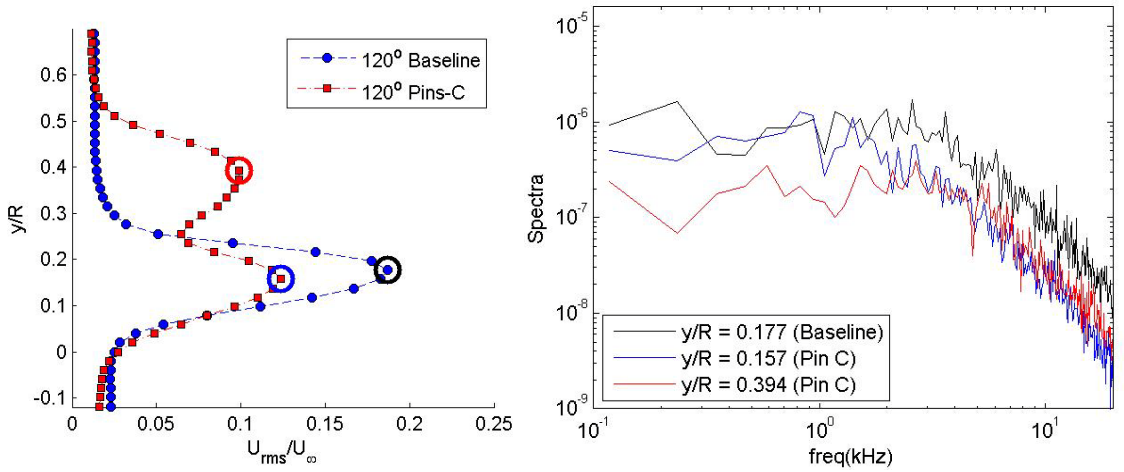

Figure 7. Left: Fluctuating velocity profiles for the baseline and the C pin configuration at *x/R* = 0.75. Right: velocity power spectra at the y-locations of the local maximum velocity fluctuations (marked by circles in the left plot) for and for the C pins configuration.

Inspection of other tested pin configurations showed that shorter pins (configurations B and E) created second shear layers which were too close to the incoming turbulent boundary layer, resulting in their merge shortly downstream of the pins, leading to a thickening of the incoming boundary layer; this effect was found to be ineffective in reducing the intensity of the main shear layer over the turret flat window. Sparse arrays of pins (configurations G and H) formed very weak second shear layers, which did not visibly affect the main shear layer.

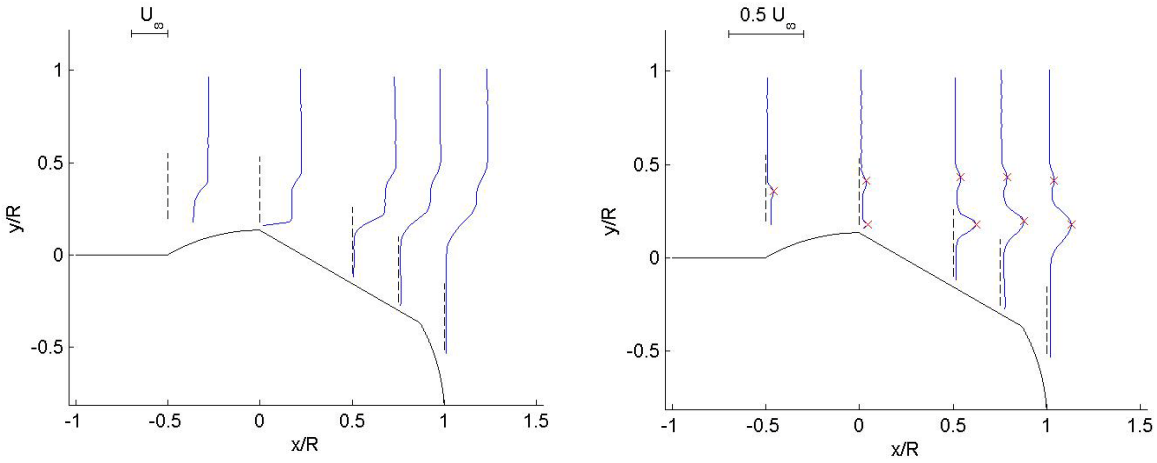

Figure 8. Normalized mean (left) and fluctuating (right) components of velocity profiles around the cylindrical turret for the F pin configuration at the elevation angle of 120 degrees. Measurement locations are marked by dashed lines. Locations of the maximum turbulent intensity are marked by crosses.

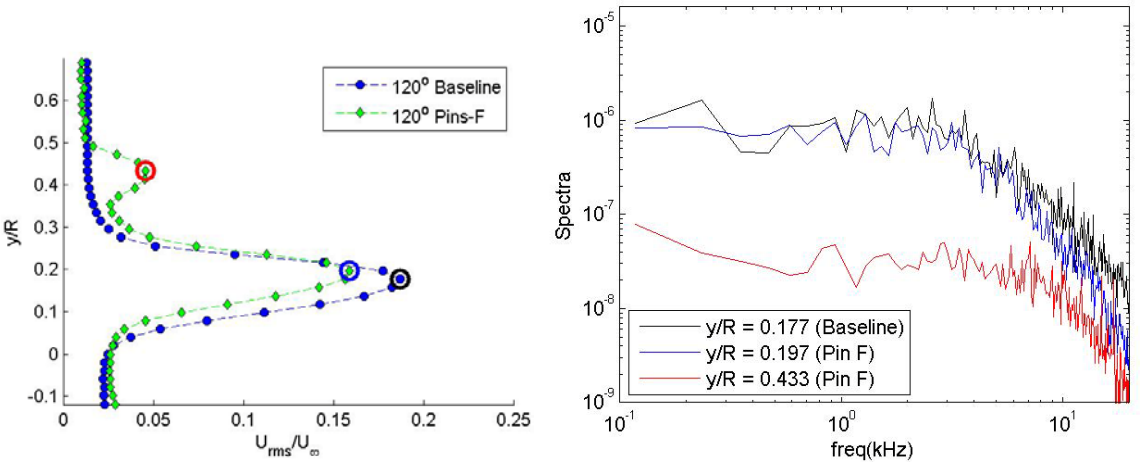

Figure 9. Left: Fluctuating velocity profiles for the baseline and the F pin configuration at x/R = 0.75. Right: velocity power spectra at the y-locations of the local maximum velocity fluctuations (marked by circles in the left plot) for and for the F pin configuration.

A. Optical Results

The reduction of the intensity of the main shear layer is potentially beneficial from an aero-optical point of view, since, depending on how it is affected, can lead to a subsequent reduction of the aero-optical aberration caused by the main shear layer. On the another hand, when the reduction is due to the formation of a second shear layer, the second shear layer will create its own aero-optical distortions, so the integrated-through-the-flow net aero-optical effect can be positive or negative depending on the intensities of both shear layers. In order to assess the potential optical benefit, direct aero-optical measurements were taken.

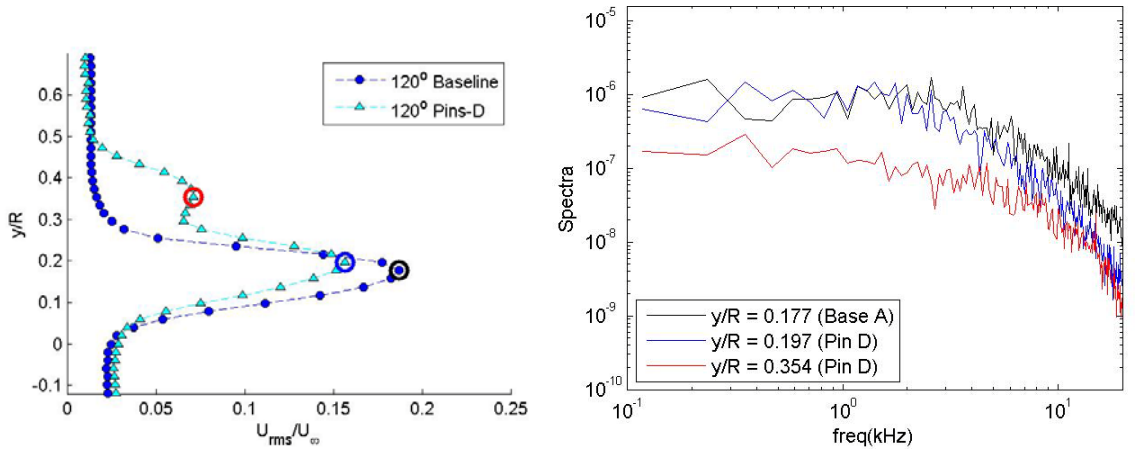

Figure 10. Left: Fluctuating velocity profiles for the baseline and the D pin configuration at x/R = 0.75. Right: velocity power spectra at the y-locations of the local maximum velocity fluctuations (marked by circles in the left plot) for and for the D pin configuration.

As mentioned above, two optical sensors were used to measure aero-optical aberrations, 2-D WaveFront Sensor (2-D WFS) and a Malley probe. The 2-D WFS was used to collect two-dimensional snapshots of instantaneous wavefronts, while the Malley probe was used to collect time series of deflection angles. From these time-series, both the amplitude spectrum and the phase between the probes' two beams were computed for each tested case. The spectrum and phase plot for the baseline case are shown in Figure 11. The hump in the amplitude spectrum, centered around 2 kHz is related to dominating large-scale structure in the shear layer at the location of the measurement [9]. The slope of the phase plot is proportional to the convective time it takes for an optically-active structure to traverse across both beams. Knowing the beams' separation, an average convective speed, U_c, (strictly speaking, the velocity component in the direction normal to the two beams) can be calculated.

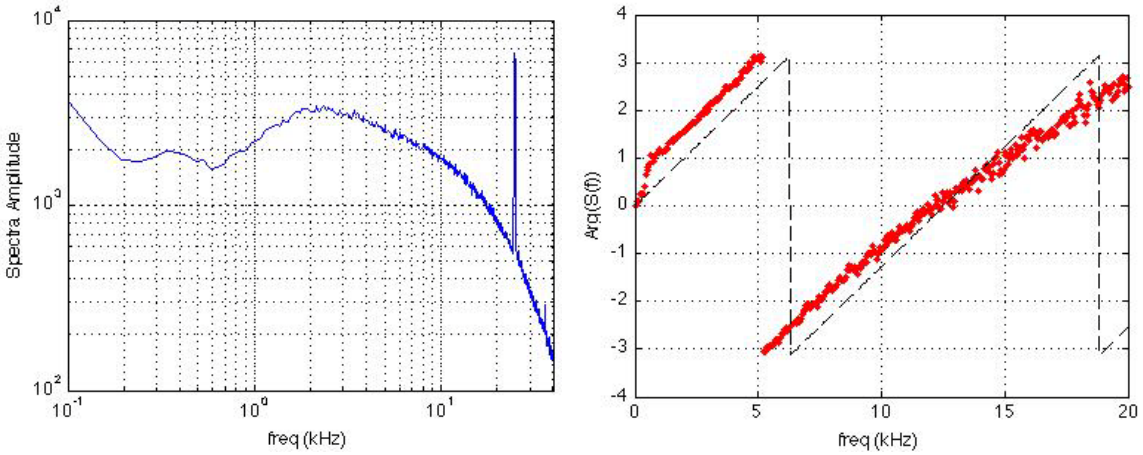

Figure 11. Malley probe amplitude spectrum (left) and phase (right) for the baseline. Linear fit is shown as a dashed line in the phase plot. M=0.5

Deflection angle spectra for the baseline and three selected pin configurations (C, D and F) for the elevation angle of 140 degrees are shown in Figure 12, left plot. At first glance, all pins decrease deflection angle spectrum, so presumably all of them should improve aero-optical environment at high elevation angles. But, it was shown in [10] the power deflection-angle spectrum is related to the level of optical distortions as,

$$OPD_{rms}^2(Ap) = U_c^2 \int_{-\infty}^{\infty} AF(Ap, f)\frac{P_\theta(f)}{(2\pi f)^2}df = U_c^2 \int_0^{\infty} G(Ap, f)P_\theta(f)df\,, \qquad [1]$$

where $G(Ap, f) = \frac{2}{(2\pi f)^2} AF(Ap, f)$ is a transfer function and $AF(Ap,f)$ is the 1-D aperture filter [11]. So, to properly compare deflection angle spectra, they need to be multiplied by the convective speed measured by the Malley probe. Investigation of the convective speeds for these pin configurations revealed that the convective speeds were consistently higher than the convective speed for the baseline, except for the configuration F, where convective speed was actually lower then for the baseline. The deflection angle spectra multiplied by the corresponding convective speed are shown in Figure 12, right plot. The velocity-multiplied deflection spectrum for configuration F was consistently lower than the baseline spectrum, so this pin configuration provides some aero-optical reductions. The spectrum for configuration D was significantly higher than the baseline spectrum in the range of frequencies between 0.5 and 2 kHz and only slightly below the baseline for frequencies above 2 kHz; therefore configuration D increases overall aero-optical distortions. It is interesting to note that the aero-optical spectrum reduction in the frequency range above 2 kHz coincides with the main-shear-layer velocity-spectrum reduction observed in Figure 10, right plot. Finally, configuration C reduced the deflection-angle spectrum in the range between 1 and 4 kHz (and also reduced the velocity-spectrum in this range, see Figure 7, right plot), but increased the deflection-angle spectrum at lower frequencies between 0.5 and 1 kHz; thus, until the actual OPD_{rms} is computed it is hard to say whether this configuration is beneficial or not.

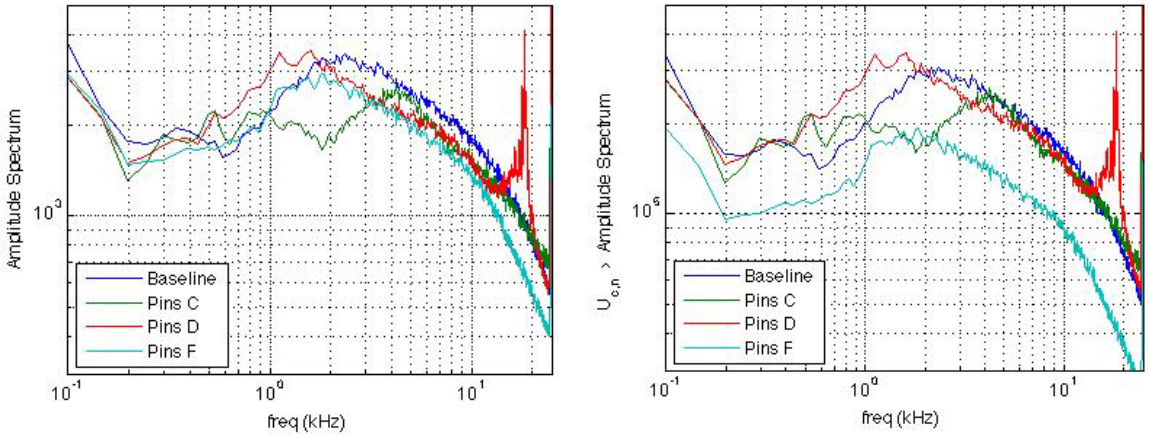

Figure 12. Left: Deflection angle spectra for selected tested cases. Right: angle spectra multiplied by the convective speed for selected tested cases. Elevation angle is 140 degrees.

Wavefronts taken by the 2-D WFS were reduced for all angles and pin configurations. Figure 13 presents the results only for 3 pin configurations, labeled Pins C, Pins D and Pins F. All results were normalized by $(\rho/\rho_{SL})M_{turret}^2 D$, where M_{turret} is the local freestream speed over the turret at x/D = 0.75 inferred from the static pressure port at that location and D is the turret diameter. Configuration C did not improve the baseline optical levels, except for 150 degrees, which will be discussed later. Configuration D, as expected from the Malley-probe analysis, made the environment worse for all angles, again except for 150 degrees. Only configuration F was found to consistently improve the aero-optical environment for all tested angles, by 15-20% for the range of angles between 120 and 145 degrees.

OPD_{rms} was also calculated from the Malley probe data using Eq [1] and the results (not shown) were found to be consistent with 2-D WFS results.

All pin configurations were found to reduce the aero-optical aberrations at 150 degrees. The flow at this angle separates over the curved surface before the turret corner and also the turret geometry at this steep elevation angle resembled a back-step configuration with a smaller, closed recirculation flow downstream of it, so aero-optical distortions of the flow are sensitive to the incoming boundary layer. All pin configurations energized the incoming boundary layer, delayed the separation over the turret and

reduced the separation region downstream of the turret, resulting in reduction of aero-optical aberrations at this angle.

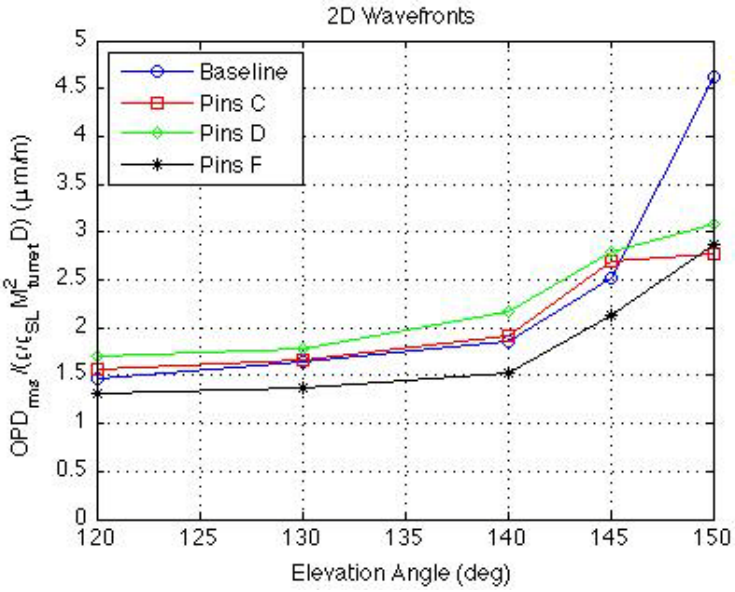

Figure 13. OPDrms for different elevation angles for the baseline and selected pin configurations measured by 2-D WFS. Incoming Mach number is 0.5.

IV. Conclusions and Discussions

As pointed out in the introduction, previous studies have shown that many pin configurations upstream of a flat-window, cylindrical turret improved the aero-optical environment for angles from 90 to 110 degrees. The mechanism for this was shown to be a simple energizing of the boundary layer so that at lower angles (90-110 degrees) the flow resisted separation at the discontinuity between the window and the cylinder. Several pin configurations with different height, spacing and diameters were tested on the cylindrical turret to see whether pins might also improve the aero-optical environment for large look-back angles (> 120 degrees). Pins with heights smaller or comparable to the thickness of the incoming boundary layer were found to just energize the boundary layer but insufficient to keep the flow attached for angles of 120 degrees or greater; the consequence was that the aero-optical distortions caused by shear layer were no better that the baseline, which also had its flow separated at the discontinuity. Pin configurations with their heights of approximately three incoming boundary-layer thicknesses introduced a second shear layer above the one associated with the incoming boundary layer; this second shear layer reduced the turbulent intensity of the main shear layer formed over the flat window. The strength of the second shear layer and the subsequent amount of the intensity reduction of the main shear layer depended on pin diameter and spacing.

In the case of configuration F, which provided the best aero-optical improvement, two shear layers were clearly separate with distinct constant velocities above and below each of them, see Figure 8. In the case of configurations C and D, the second shear layer was strong enough to start directly interacting with the main shear layer, see Figure 6 and Figure 10, left plot.

To better understand why configuration F reduced aero-optical aberrations, it is necessary to revisit the relation between the flow parameters and aero-optical distortions. In [12] the "linking equation" between turbulence quantities and optical phase variance was developed as $OPD_{rms}^2 = 2K_{GD}^2 \int_0^L \sigma_{\rho'}^2 \Lambda_\rho(\zeta) d\zeta$, where K_{GD} is the Gladstone-Dale constant (which for air and visible wavelengths is approximately 2.27×10^{-4} m^3/kg), $\sigma_{\rho'}$ is the mean-squared density variance, Λ_ρ is the density correlation length and the integration is performed along the laser beam direction, ζ. Neglecting pressure fluctuations inside the shear layer, it is possible to re-write the linking equation as [13],

$$\mathrm{OPD}_{\mathrm{rms}} = A\delta\frac{\rho_\infty}{\rho_{SL}}M^2,\ \text{where}\ A=\sqrt{2}K_{GD}\rho_{SL}(\gamma-1)\left[\int_0^\infty\left[\left(\frac{U(\varsigma)u_{\mathrm{rms}}(\varsigma)}{U_\infty^2}\right)^2\frac{\Lambda_\rho(\varsigma)}{\delta}\right]d(\varsigma/\delta)\right]^{1/2}, \quad [2]$$

where γ = 1.4 and δ is the characteristic shear layer thickness. This integral can be evaluated using the velocity values in the middle of the shear layer and assuming that $\Lambda_\rho \sim \delta$, so Eq. [2] can be further simplified (for a fixed M) as

$$\mathrm{OPD}_{\mathrm{rms}} \sim \overline{U}\cdot u_{rms}^{(\max)}\cdot\delta, \quad [3]$$

where $\overline{U}=0.5(U_{upper}+U_{lower})$ is the mean convective speed, defined by the velocities above, U_{upper}, and below, U_{lower}, the shear layer and $u_{rms}^{(\max)}$ is the maximum value of fluctuating component in the shear layer. The local shear layer thickness can be estimated using the linear model for incompressible shear layer growth [14], $\frac{d\delta}{dx}\sim\frac{U_{upper}-U_{lower}}{U_{upper}+U_{lower}}=2\frac{\Delta U}{\overline{U}}$, with $\Delta U = U_{upper}-U_{lower}$, the velocity deficit across the shear layer; integrating over the streamwise distance of L gives $\delta\sim\frac{\Delta U}{\overline{U}}L$. Also, the maximum value of the velocity fluctuation is proportional to ΔU [15], $u_{rms}^{(\max)}\sim\Delta U$. Substituting all these quantities into Eq. [3], the final equation of the level of aero-optical distortions caused by the shear layer can be written as,

$$OPD_{rms}\sim(\Delta U)^2 L \quad [4].$$

In the case in two *non-interacting* shear layers the overall level of aero-optical aberrations is the geometric mean of each individual shear layer,

$$OPD_{rms}=\left[OPD_{rms}^2(SL1)+OPD_{rms}^2(SL2)\right]^{1/2}\sim\left[(\Delta U_1)^4L_1^2+(\Delta U_2)^4L_2^2\right]^{1/2} \quad [5]$$

where $\Delta U_1 = \Delta U - \Delta U_2$ and ΔU_2 are defined in Figure 14, left. The reduction in OPD_{rms} can be finally re-written as a function of the normalized upper-shear-layer velocity difference, $\Delta U_2/\Delta U$ as,

$$\frac{OPD_{rms}}{OPD_{rms}^{(baseline)}}=\frac{\left\{\left[1-(\Delta U_2/\Delta U)\right]^4L_1^2+(\Delta U_2/\Delta U)^4L_2^2\right\}^{1/2}}{L_1} \quad [6]$$

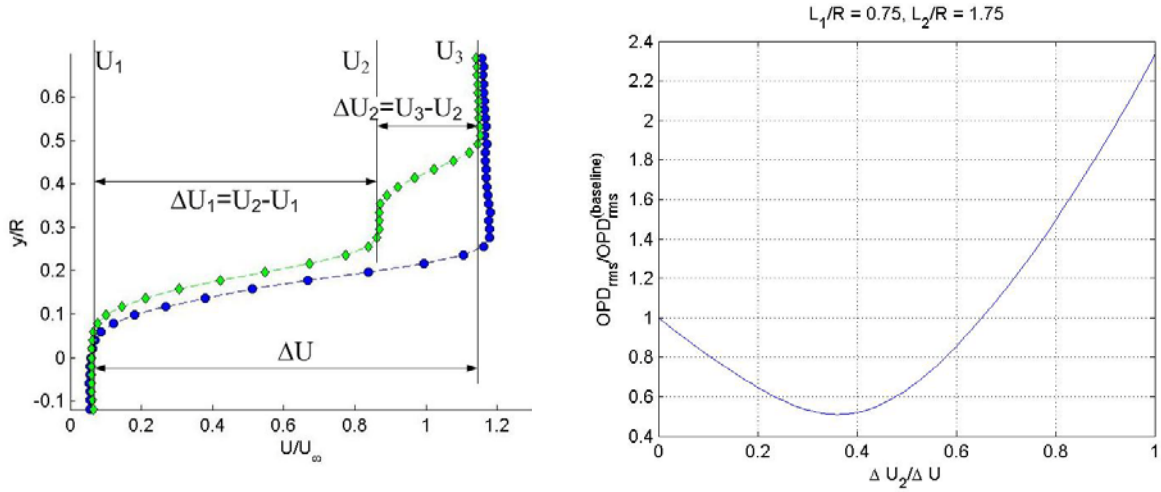

Figure 14. Left: Definition of two-shear-layer flow. Right: results of modeling, Eq [6].

If we assume that the upper shear layer started at the location of pins and the main shear layer started at the turret corner, by the streamwise location x/R = 0.75 (since the laser beam crossed the shear layer approximately at this location) L_1 = 0.75R and L_2 = 1.75R. Using these parameters, Eq. [6] is plotted in Figure 14, right plot. The $\mathrm{OPD}_{\mathrm{rms}}$ decreases for small ΔU_2, has the minimum at $\Delta U_2/\Delta U$ = 0.35 and increases for larger upper-shear-layer velocity deficits. From Figure 8, the experimental value for the velocity deficit for configuration F was found to be $\Delta U_2/\Delta U$ = 0.27, which is close to the model-predicted optimal velocity deficit. Also, the model assumes that the main-shear-layer thickness is proportional to

ΔU_1, implying that it should be smaller for the configuration F that for the baseline; indeed, this effect can be clearly observed in Figure 9, left plot.

Of course, this model gives mostly qualitative trends, since it is based on several over-simplifying assumptions; nevertheless, it correctly predicts the decrease in OPD_{rms} and provides plausible physical explanation for aero-optical reduction. The model assumes that two shear layers do not interact over the flat window, which is clearly not the case for configurations C and D, as both shear layers started merging before x/R = 0.75. The shear layer interaction increases the shear layer thickness and the turbulent intensity, inevitably increasing the correlation lengths and u_{rms} and resulting aero-optical distortions, according to the linking equation.

Based on the reasoning leading to the model, the strategy for reducing the aero-optical distortions over the two-dimensional turret with the flat window using pins is to create a small-diameter, partial blockage by placing series of small tall (~ 3 incoming BL thickness) pins on the floor upstream of the turret. The small blockage creates a weak shear layer above the main shear layer and reduces the upper speed of the main shear layer, thus reducing the level of velocity fluctuations and thereby reducing the aero-optical distortions imposed by the main shear layer. The second shear layer should be strong enough to reduce the upper velocity over the main shear layer, but not so strong as to start interacting with the main shear layer, which would result in the increase of turbulence levels inside the second shear layer. Now that the model exists from which a strategy emerges, new configurations beg to further investigation to test the validity of the model.

References

[1] S. Gordeyev and E. Jumper, “Fluid Dynamics and Aero-Optics of Turrets”, submitted to *Progress in Aerospace Sciences*, 2010.

[2] Gilbert, K. G. and Otten L. J. (eds), ``Aero-Optical Phenomena," *Progress in Astronautics and Aeronautics*, Vol. 80, pp. 1-9, AIAA, New York, 1982.

[3] S. Gordeyev, T. Hayden and E. Jumper, "Aero-Optical and Flow Measurements Over a Flat-Windowed Turret", *AIAA Journal*, vol. **45**, No. 2, pp. 347-357, 2007.

[4] E. J. Fitzgerald and E. J. Jumper, ``The Optical Distortion Mechanism in a Nearly Incompressible Free Shear Layer," *Journal of Fluid Mechanics*, Vol. **512**, pp. 153-189, 2004.

[5] S. Gordeyev, J.A. Cress, E. Jumper and A.B. Cain,”Aero-Optical Environment Around a Cylindrical Turret with a Flat Window,” submitted to *AIAA Journal*, 2010.

[6] S. Gordeyev, E. Jumper, T. Ng and A. Cain, "The Optical Environment of a Cylindrical Turret with a Flat Window and the Impact of Passive Control Devices", 36th AIAA Plasmadynamics and Laser Conference, Toronto, Canada, 6-9 June, 2005, AIAA Paper 2005-4657.

[7] J. Cress, S. Gordeyev, E. Jumper, T. Ng and A. Cain, "Similarities and Differences in Aero- Optical Structure over Cylindrical and Hemispherical Turrets with a Flat Window", 45th Aerospace Science Meeting and Exhibit, Reno, Nevada, 8-11 Jan, 2007, AIAA Paper 2007-0326.

[8] Jumper, E.J., and E.J. Fitzgerald, “Recent Advances in Aero-Optics”, *Progress in Aerospace Sciences*, **37**, 2001, pp.299-339.

[9] A. M. Nightingale, S. Gordeyev and E. J**.** Jumper,” Optical Characterization of a Simulated Weakly-Compressible Shear Layer: Unforced and Forced,” *AIAA Journal*, Vol. **47**, No. 10, Oct. 2009, pp. 2298-2305.

[10] B. Vukasinovic, A. Glezer, S. Gordeyev, E. Jumper and V. Kibens, "Fluidic Control of a Turret Wake: Aerodynamic and Aero-Optical Effects", accepted to *AIAA Journal*, 2010.

[11] Siegenthaler, J., Gordeyev, S., and Jumper, E., “Shear layers and aperture effects for aero-optics", *AIAA Paper* 2005-4772, 2005.

[12] Sutton, G.W., “Effect of Turbulent Fluctuations in an Optically Active Fluid Medium,” *AIAA Journal*, Vol. 7, No. 9, September 1969, pp. 1737-1743.

[13] J. Cress, S. Gordeyev and E. Jumper, "Aero-Optical Measurements in a Heated, Subsonic, Turbulent Boundary Layer" , 48th Aerospace Science Meeting and Exhibit, Orlando, Florida, 4-7 Jan, 2010, AIAA Paper 2010-0434.

[14] Brown, G. L. and Roshko, A,”On density effects and large structure in turbulent mixing layers”, *J. Fluid Mech.* **64**, pp. 775-816. 1974.

[15] Rogers, M. M. and Moser, R. D.,”Direct simulation of a self-similar turbulent mixing layer”, *Phys. Fluids*, **6**, pp. 903-923, 1994.